Structural and Magnetic Properties of $Cr_{1+t}Sb_{1-x}Te_x$

P. H. Andresen,[a] H. Fjellvåg,[a] A. Kjekshus[a,*] and O. Steinsvoll[b]

[a]Department of Chemistry, University of Oslo, N-0315 Oslo 3, Norway and [b]Institute for Energy Technology, N-2007 Kjeller, Norway

Andresen, P. H., Fjellvåg, H., Kjekshus, A. and Steinsvoll, O., 1993. Structural and Magnetic Properties of $Cr_{1+t}Sb_{1-x}Te_x$. – Acta Chem. Scand. 47: 264–270.

$Cr_{1+t}Sb_{1-x}Te_x$ has been investigated for $0.00 \leqslant x \leqslant 0.50$ for the series $CrSb_{1-x}Te_x$ and $Cr_{1.05}Sb_{1-x}Te_x$ by powder X-ray and neutron diffraction, DSC and magnetic susceptibility measurements. $Cr_{1+t}Sb_{1-x}Te_x$ takes the NiAs-type structure. $Cr_{1+t}Sb_{1-x}Te_x$ has a homogeneity range on the Cr-rich side, here only examined for $t = 0.05$, which, however, nearly coincides with the upper limit. For increasing x, the homogeneity range narrows, and the metal enrichment is probably absent for $x > \sim 0.20$. The Curie–Weiss law is satisfied for all samples in the high-temperature paramagnetic regime. The cooperative magnetic state changes from typically antiferromagnetic for $x = 0.00$ to ferromagnetic-like for $x = 0.50$. A slight reduction in the Néel temperature is observed for the $t = 0.05$ series when $x < \sim 0.20$. The antiferromagnetic structure for $t = 0.00$ and $x = 0.00$, 0.10 and 0.20 has been determined from powder neutron diffraction. On increasing x, T_N is reduced from 680 K for $x = 0.00$ to 180 K for $x \approx 0.50$. For $\sim 0.15 \leqslant x \leqslant \sim 0.50$ more than one cooperative state (antiferro- and canted magnetic arrangements) exist at low temperatures. The magnetic phase diagram for $0.00 \leqslant x \leqslant 0.50$ is reconsidered.

Previous studies[1-4] have shown that CrSb and CrTe form a continuous solid solution phase $Cr_{1+t}Sb_{1-x}Te_x$, where the stoichiometry may deviate from the ideal metal : non-metal ratio of 1 : 1. The crystal structure is of the NiAs type over the entire composition range $0.00 \leqslant x \leqslant 1.00$. The magnetic phase diagram for $Cr_{1+t}Sb_{1-x}Te_x$ shows a number of interesting features. Whereas CrSb is antiferromagnetic,[1-8] CrTe is ferromagnetic[1-4,9] at low temperatures. At least two, somewhat different, magnetic phase diagrams are reported.[2-4] The main difference concerns the region around $x = 0.50$, and is connected with whether there occurs one single phase[2,3] with a canted magnetic structure or a magnetic two-phase[4] situation with a canted and a ferrimagnetic phase.

The homogeneity range with respect to the metal content has so far only been studied for the binary end members of the solid-solution phase. Whereas CrSb has a homogeneity range on the metal-rich side, it occurs on the non-metal rich side for CrTe.[10-13] In the present report, the properties of $Cr_{1+t}Sb_{1-x}Te_x$ are studied for $0.00 \leqslant x \leqslant 0.50$ within the range of homogeneity with respect to t. Magnetic properties and phase transitions are studied by means of magnetic susceptibility, magnetization, differential scanning calorimetry (DSC), high- and low-temperature powder X-ray diffraction and neutron diffraction experiments. The results are discussed in relation to earlier knowledge on the CrSb–CrTe system.

Experimental

The pure elements [Cr pieces (99.99%), Sb lumps (99.999%) and Te lumps (99.999%), all Koch-Light Laboratories Ltd.] were used as starting materials for the syntheses of $Cr_{1+t}Sb_{1-x}Te_x$ samples. Accurately weighed amounts of the components were heated in evacuated, sealed silica-glass capsules. The samples were heated repeatedly (2–6 times, increasing with increasing x) at 950°C for 2–3 weeks, then at 800°C for 3 days before being slowly cooled (during 1 day) to room temperature. The samples were carefully crushed between each heating cycle. After the last annealing cycle, the samples were quenched in ice water from 800°C.

All samples were characterized by room-temperature powder X-ray diffraction (PXD; Guinier Hägg cameras, $CuK\alpha_1$ radiation and Si as internal standard). For a few samples one faint PXD line from a Cr_2O_3 impurity was observed. Position and intensity measurements of the reflections were carried out using a Nicolet L18 microdensitometer controlled by the SCANPI program system.[14] Low- and high-temperature PXD experiments were carried out between 120 and 1100 K, using an Enraf–Nonius (FR 553) Guinier Simon camera ($CuK\alpha_1$ radiation). The samples were contained in rotating sealed, thin-walled silica-glass capillaries. A Pt-resistance thermometer was used in the temperature regulation. Least-squares refinements for deducing unit cell dimensions were performed with the CELLKANT program.[15]

Powder neutron diffraction (PND) experiments were collected with the OPUS III two-axis diffractometer at the JEEP II reactor, Kjeller. Monochromatized neutrons

* To whom correspondence should be addressed.

of wavelength 187.7 pm were obtained by reflection from (111) of a Ge crystal, and diffraction data were collected between $2\Theta = 5$ and 100° in steps of 0.05°. The temperature was varied between 10 and 300 K using a Displex cooling device, and the temperature was controlled and regulated within ±0.5 K by means of a Thor 3010 controller. PND experiments between 300 and 700 K were performed in an oven with separate temperature regulation of the upper and lower part, and the temperature difference was kept within ±1 K. During the latter experiments the samples were kept inside evacuated, sealed silica-glass ampoules. The Hewat version[16] of the Rietveld program[17] was used in fitting instrumental and structural parameters. The scattering lengths $b_{Cr} = 3.635$, $b_{Sb} = 5.641$ and $b_{Te} = 5.43$ fm were taken from Ref. 18, and magnetic form factors for Cr^{3+} from Ref. 19.

DSC were performed between 110 and 870 K using a Mettler TA 3000 system at a heating rate of 10 K min^{-1}. Data reduction was performed with standard programs for the system. Magnetic susceptibility measurements were carried out between 77 and 950 K according to the Faraday method (maximum field 8 kG, 5–20 mg samples). Magnetic susceptibility and magnetization data were collected between 4 and 300 K using a SQUID magnetometer (Quantum Design, applied fields 50–500 G).

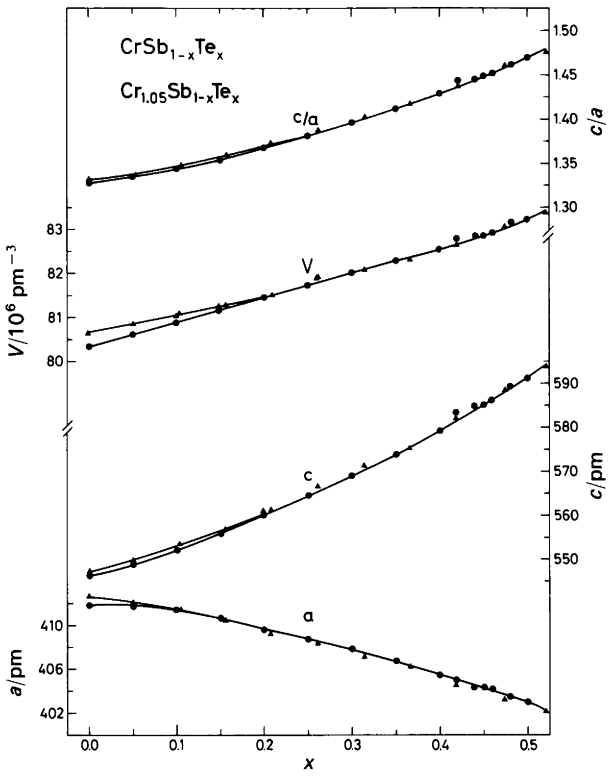

Fig. 1. Unit cell dimensions for $CrSb_{1-x}Te_x$ (●) and $Cr_{1.05}Sb_{1-x}Te_x$ (▲) for $0.00 \leqslant x \leqslant 0.50$. Calculated errors do not exceed size of symbols.

Results and discussion

Structural properties. The variation of the unit cell dimensions for samples of $CrSb_{1-x}Te_x$ and $Cr_{1.05}Sb_{1-x}Te_x$ with x is given in Fig. 1. The curve for $t = 0.00$ fits earlier results well,[1-3] and the structure is of the simple NiAs type over the entire composition range. The Sb and Te atoms proved from PND-based profile refinements to be randomly (long-range) distributed over the non-metal position. Comparison of the two sets of unit cell data, and in particular the volume V, in Fig. 1, shows that the volumes coincide for $x > \sim 0.20$, which clearly suggests that the homogeneity region on the metal-rich side exists only at low Te-substitution levels, viz. $x < 0.20$. The partial filling-up of the trigonal bipyramidal holes of the NiAs-type structure of $Cr_{1.05}Sb_{1-x}Te_x$ was ascertained by powder neutron diffraction studies for $x = 0.00$, 0.10 and 0.20, and is consistent with earlier findings for $Cr_{1+t}Sb$.[11]

Representative thermal expansion curves for $CrSb_{1-x}Te_x$ are shown in Fig. 2. For CrSb (Fig. 2a) a marked, but continuous volume change occurs in the $V(T)$ curve between 600 and 700 K (see also Ref. 6). The structural changes are directly coupled to the transition between para- (P) and antiferro- (AF) magnetic states [see below, and the Néel temperature (T_N) marked on the illustration]. The effect is strongly anisotropic, involving a large contraction of the c-axis in the AF phase coupled with a substantial magnetostrictive expansion of the a-axis. Close inspection of the Guinier Simon films taken over a limited temperature interval reveal that the structural changes are continuous. These features are also found for $0.00 < x < 0.50$ in Fig. 2b–2e, but with a decreasing magnetostrictive effect with increasing Te content. At the same time (Fig. 2), T_N is gradually shifted towards lower temperatures.

Magnetic susceptibility, magnetic structure and phase diagram. The inverse magnetic susceptibility versus temperature curves for $CrSb_{1-x}Te_x$ and $Cr_{1.05}Sb_{1-x}Te_x$ are shown in Fig. 3. In the paramagnetic regime at high temperatures all samples exhibit Curie–Weiss law behaviour. The paramagnetic moment for CrSb is $\mu_p = (4.4 \pm 0.2)\mu_B$. On increasing the Te content, μ_p remains fairly constant up to $x = 0.20$ and then decreases slightly to $(3.9 \pm 0.1)\mu_B$ for $x = 0.50$. However, a rather large variation is found for the Weiss constant (Θ), which is increased from -430 ± 80 K for CrSb to 215 ± 10 K for $CrSb_{0.50}Te_{0.50}$; the change in sign occurs at $x \approx 0.20$.

There is no major difference in magnitude or in the composition (x) dependence for the paramagnetic moment of the studied samples of $CrSb_{1-x}Te_x$ and $Cr_{1.05}Sb_{1-x}Te_x$. On the other hand, for $0.00 \leqslant x < \sim 0.20$, Θ increases with increasing metal content (e.g. for $x = 0.05$: $\Theta = -300 \pm 25$ for $t = 0.00$, and $\Theta = -225 \pm 35$ K for $t = 0.05$). A similar feature is also reflected in Fig. 4, which shows the variation of T_N over the composition range $0.00 \leqslant x \leqslant \sim 0.20$. Fig. 4 moreover

serves to illustrate the good mutual consistency between the different determinations of T_N.

The low-temperature part of the $\chi^{-1}(T)$ curve for CrSb in Fig. 3a (Faraday balance measurements) indicates antiferromagnetic interactions. The onset of antiferromagnetism, as judged from the $\chi^{-1}(T)$ data in Fig. 3, complies well with the thermal expansion features discussed above (Fig. 2). For Te-substituted samples there is a tendency towards increasing susceptibility at low temperatures, thereby reducing the low-temperature maxima on the $\chi^{-1}(T)$ curves in Fig. 3. This suggests that ferromagnetic couplings become more dominant for samples with higher Te content. This complies with the fact that indirect exchange interactions are considered to be strong for $CrSb_{1-x}Te_x$, being negative for Cr–Sb–Cr and positive for Cr–Te–Cr.

Low-temperature magnetic susceptibility curves are shown for selected samples in Fig. 5 and should be considered in relation to the high-temperature $\chi^{-1}(T)$ data in Fig. 3. Note that the entire temperature range for some of the curves in Fig. 5 is well below T_N. A distinct change in the curves occurs on increasing the Te content. On going from $x = 0.15$ to 0.50, the susceptibility at 5 K increases by almost three orders of magnitude. For $x = 0.15$, the low susceptibility and its rather subtle increase at low temperature point at an almost perfect antiferromagnetic order (i.e. no canting). For $x = 0.25$, the marked low-temperature increase in χ suggests additional, weak ferromagnetism. For $x = 0.40$ and 0.50, the ferromagnetic contribution becomes larger. The drop in $\chi(T)$ for $x = 0.50$ at round 90 K indicates a transition between two different, but mainly ferromagnetic regimes.

With a basis in the present susceptibility measurements, the magnetic phase diagram for $CrSb_{1-x}Te_x$ in Fig. 6 is forwarded for $0.00 \leqslant x \leqslant 0.50$. At least three different regions with cooperative magnetism may be defined; an antiferromagnetic region (AF1) containing CrSb and having a broad extension at higher temperatures, another mainly antiferromagnetic region (AF2) at low temperatures, and one or possibly two canted-/ferromagnetic regions (C1 and C2) for the most Te-rich part covered in this study. Labelling of the phase boundaries is given on the illustration.

Previous investigations have proposed two somewhat different magnetic phase diagrams for $CrSb_{1-x}Te_x$.[2-4] According to the double exchange model (see e.g.

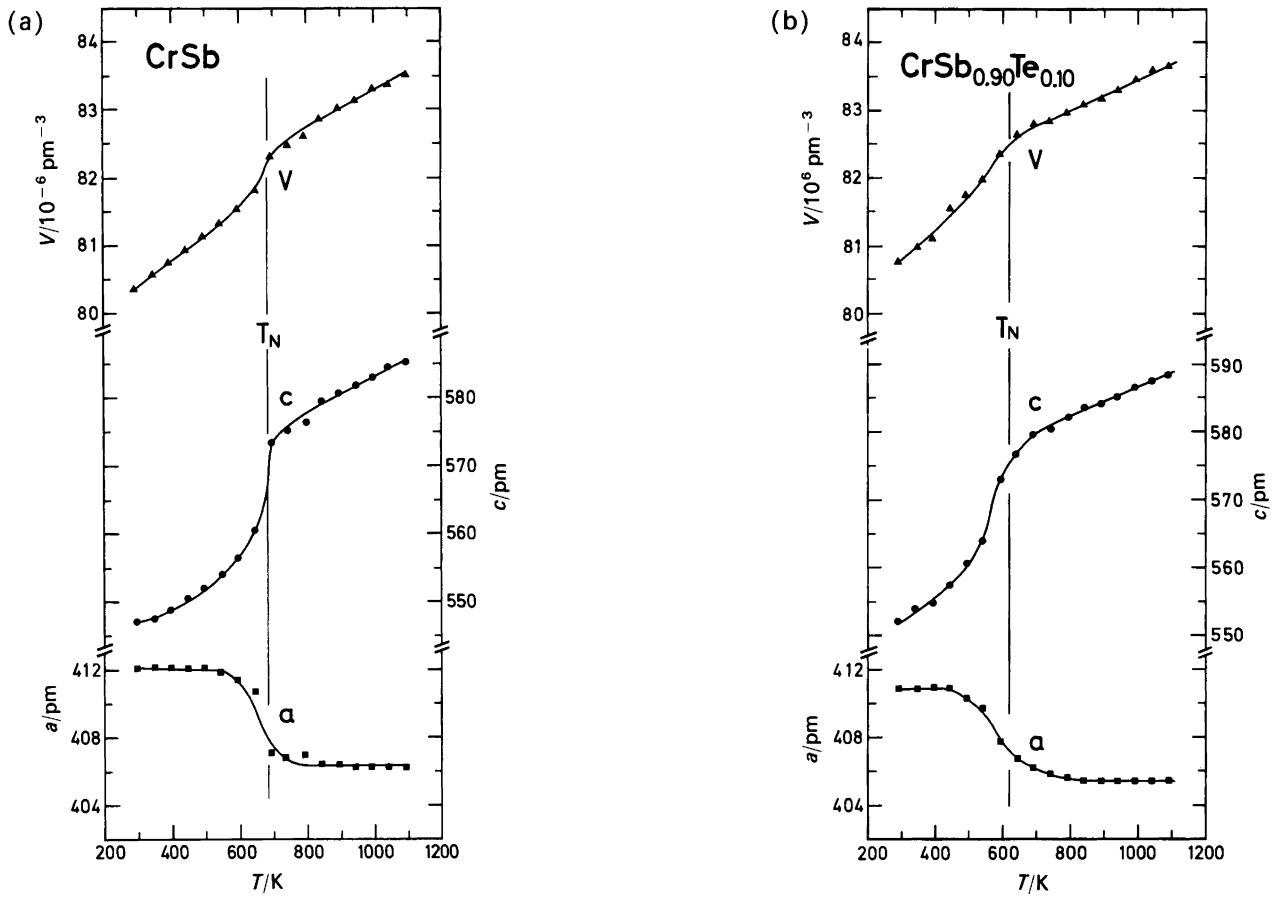

Fig. 2. Variation of unit cell dimensions with temperature for $CrSb_{1-x}Te_x$ with (a) $x = 0.00$, (b) 0.10, (c) 0.20, (d) 0.30 and (e) 0.40. Calculated errors do not exceed size of symbols. T_N as determined by magnetic susceptibility measurements are marked.

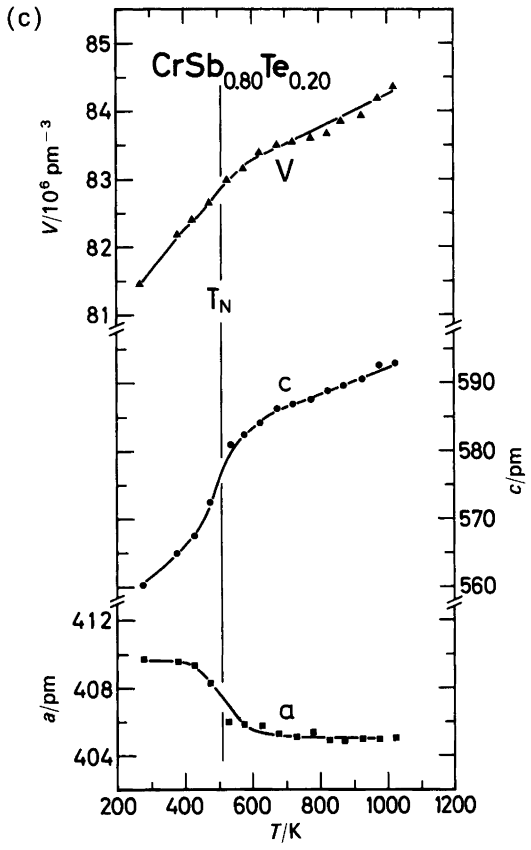

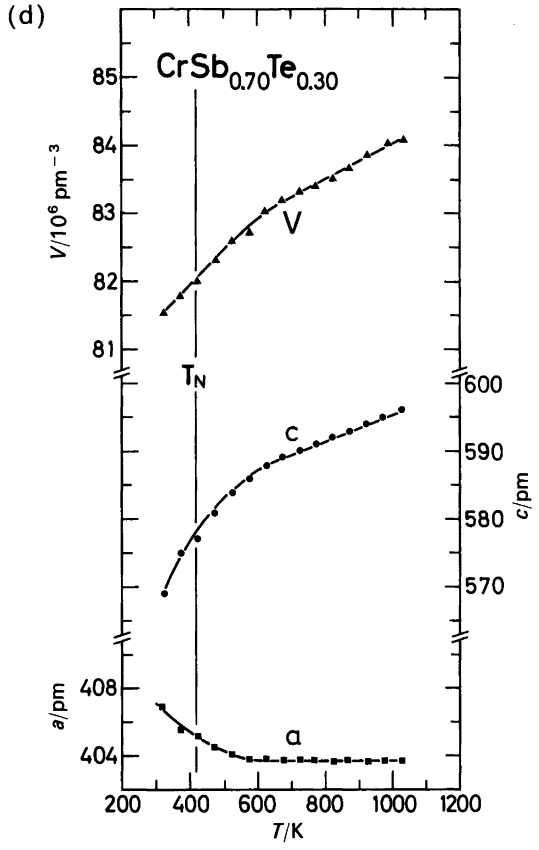

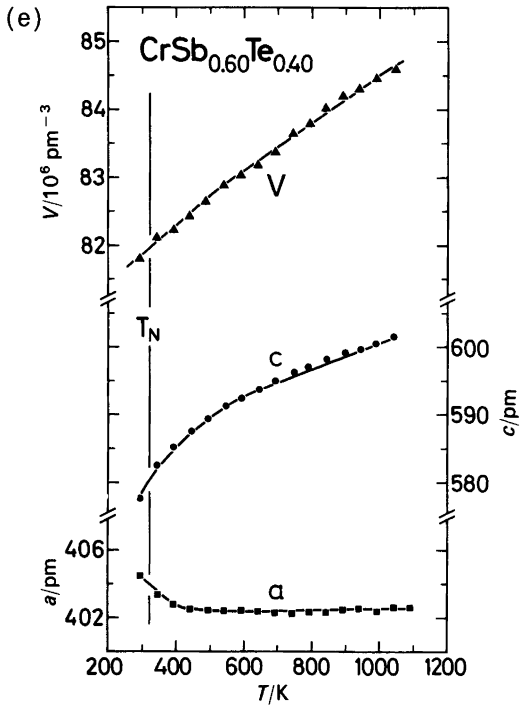

Fig. 2. Continued.

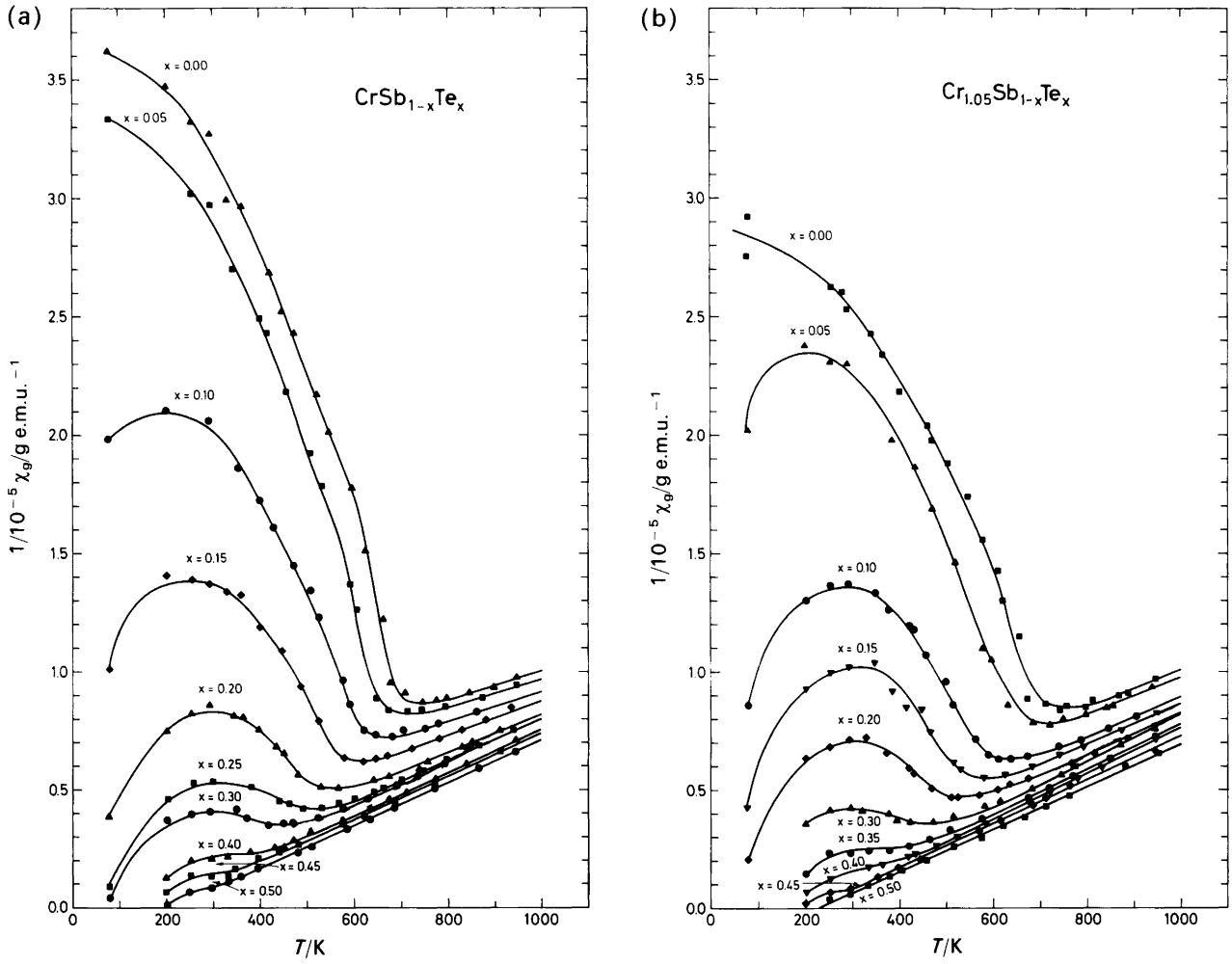

Fig. 3. Inverse magnetic susceptibility versus temperature for (a) $CrSb_{1-x}Te_x$ and (b) $Cr_{1.05}Sb_{1-x}Te_x$ ($0.00 \leqslant x \leqslant 0.50$) between 80 and 920 K as determined by the Faraday technique.

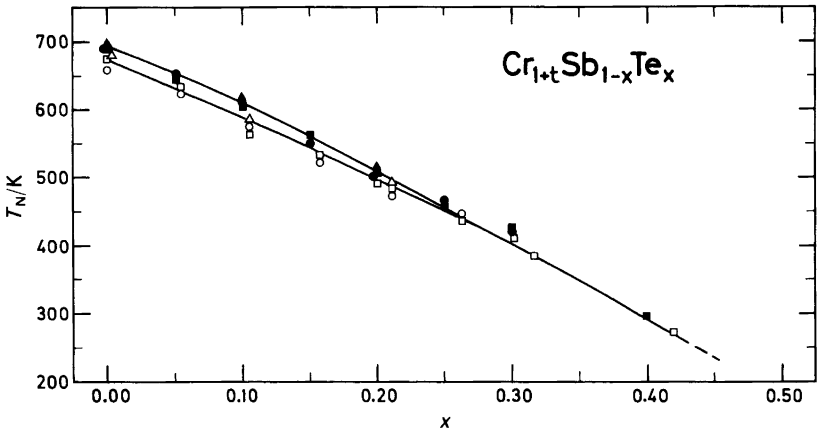

Fig. 4. Composition variation of T_N for $CrSb_{1-x}Te_x$ (filled symbols) and $Cr_{1.05}Sb_{1-x}Te_x$ (open symbols). Experimental points: (●,○) magnetic susceptibility, (▲,△) high-temperature PXD, (■,□) DTA and (◆,◇) PND.

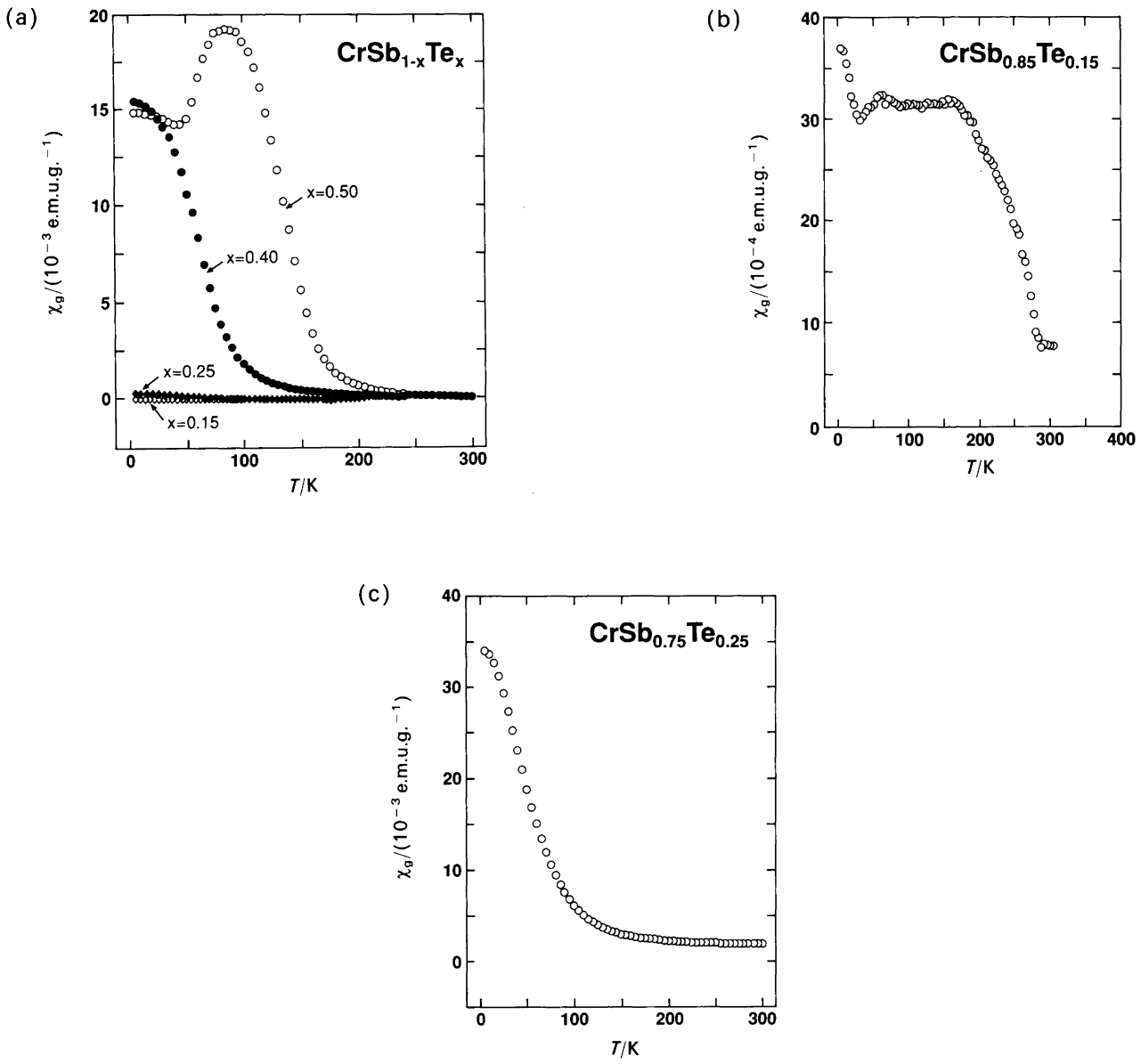

Fig. 5. Temperature variation in magnetic susceptibility between 5 and 320 K for $CrSb_{1-x}Te_x$: (a) $x=0.15$, 0.25, 0.40 and 0.50, (b) $x=0.15$ and (c) $x=0.25$ as determined by SQUID measurements.

Refs. 20–22), the substitution is expected to give rise to different Cr valence states, and electrons may move between the states. The total energy of the magnetic system will depend on the orientations of the magnetic moments, and according to the theoretical considerations by de Gennes,[22] the cooperative magnetic state of $CrSb_{1-x}Te_x$ should represent a magnetic one-phase region where the antiferro- and ferromagnetic components of the canted structure may vary both with composition and temperature. The predicted magnetic phase diagram by de Gennes is essentially consistent with the experimentally founded diagram by Cox *et al.*[2,3] However, this proposal is not in accordance with the observations in Figs. 5 and 6, nor with the results of Grazhdankina and Zainullina.[4] The latter authors propose the existence of antiferro-, ferro-, ferri-, canted and mixed ferri- and canted magnetic phase fields, and although deviating considerably with respect to details, their interpretation is more in line with the present data.

From powder neutron diffraction experiments (10–700 K) more information on the magnetic ordering was obtained for $Cr_{1.05}Sb$, $Cr_{1.05}Sb_{0.90}Te_{0.10}$, $Cr_{1.05}Sb_{0.80}Te_{0.20}$, CrSb, $CrSb_{0.90}Te_{0.10}$ and $CrSb_{0.80}Te_{0.20}$. Upon cooling below T_N, the magnetic reflection 111 [extinguished crystallographically for the NiAs-type structure (*hhl* absent for $l=2n+1$; $P6_3/mmc$)], appeared. All reflections were indexable on a simple NiAs-type unit cell.

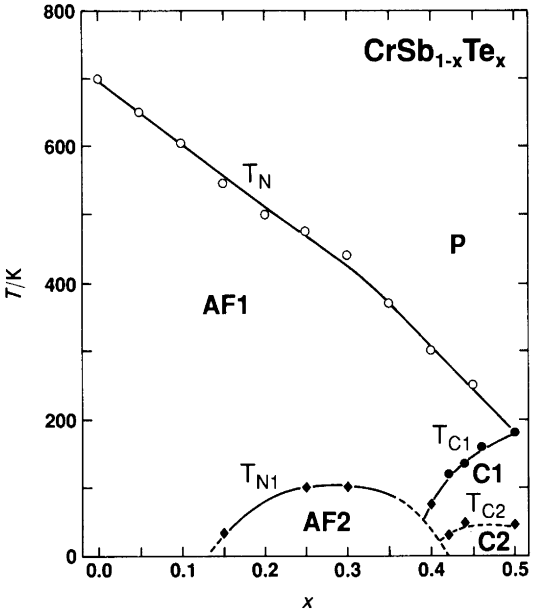

Fig. 6. Magnetic phase diagram for $CrSb_{1-x}Te_x$: $0.00 \leqslant x \leqslant 0.50$ (AF antiferro-, C canted antiferro-, P paramagnetic).

The presence of (111) in the room-temperature PND diagrams for $x = 0.00$, 0.10 and 0.20 immediately suggests antiferromagnetic order along the c-axis (alternate moment planes through atoms at 0,0,0 and 0,0,1/2). This complies fully with earlier reports on CrSb[1-8] (cf. also the phase diagram in Fig. 6). The magnetic moments were found to be parallel to the c-axis at room temperature, and the moment $\mu_{AF} = (2.8 \pm 0.1)\mu_B$ was found to be virtually constant between 10 and 300 K, and for

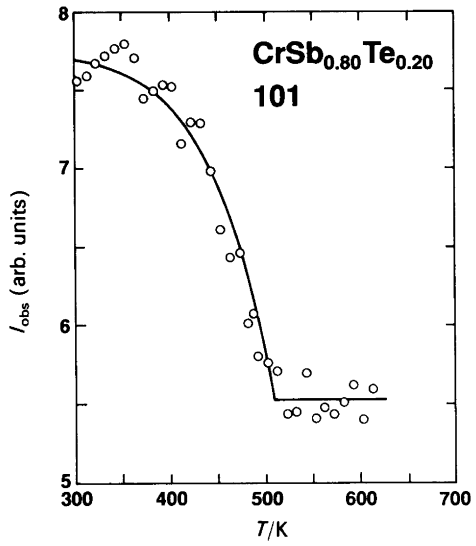

Fig. 7. Temperature dependence of integrated intensity of 101 reflection between 300 and 650 K for $CrSb_{0.80}Te_{0.20}$.

$0.00 \leqslant x \leqslant 0.20$. The overall temperature variation of the integrated intensity of the magnetic contribution to the 101 reflection for $CrSb_{0.80}Te_{0.20}$ between 300 and 650 K in Fig. 7 fits the picture of a second-order phase transition at T_N.

The temperature dependence of the integrated intensities of the purely magnetic and the fundamental reflections should convey information on possible magnetic order–order transitions connected with a turning of the moments from parallel to perpendicular to c (viz. within the basal ab-plane). However, none of such temperature dependences examined in this study showed any sign of anomaly in the temperature range 10–110 K. Hence the anomalies in the magnetic susceptibility (see Figs. 5 and 6) could not be verified from PND data as perturbation(s) of the antiferromagnetic structure.

References

1. Lotgering, F. K. and Gorter, A. W. *J. Phys. Chem. Solids 3* (1957) 238.
2. Cox, D. E., Shirane G. and Takei, W. J. *Proc. Int. Conf. Magnetism*, Nottingham 1964 (Inst. Phys. Soc., London 1965) p. 291.
3. Takei, W. J., Cox, D. E. and Shirane, G. *J. Appl. Phys. 37* (1966) 973.
4. Grazhdankina, N. P. and Zainullina, R. I. *Zh. Exp. Teor. Fiz. 59* (1970) 1896 [*Sov. Phys. JETP 32* (1971) 1025].
5. Snow, A. I. *Phys. Rev. 85* (1952) 365.
6. Snow, A. I. *Rev. Mod. Phys. 25* (1953) 127.
7. Tsubokawa, I. *J. Phys. Soc. Jpn. 16* (1961) 277.
8. Takei, W. J., Cox, D. E. and Shirane, G. *Phys. Rev. 129* (1963) 2008.
9. Hirone, T. and Chiba, S. *J. Phys. Soc. Jpn. 15* (1960) 1991.
10. Williams, R. S. *Z. Anorg. Chem. 55* (1907) 1.
11. Kjekshus, A. and Walseth, K. P. *Acta Chem. Scand. 23* (1969) 2621.
12. Foëx, G. and Graff, M. *C. R. Acad. Sci. 209* (1939) 160.
13. Ipser, H. Komarek, K. L. and Klepp, K. O. *J. Less-Common Met. 92* (1983) 265.
14. Werner, P. E. *The Computer Program SCANPI*, Institute of Inorganic Chemistry, University of Stockholm, Stockholm, Sweden 1981.
15. Ersson, N. O. *Program CELLKANT*, Institute of Chemistry, Uppsala University, Uppsala, Sweden 1981.
16. Hewat, A. W. *The Rietveld Computer Program for the Profile Refinement of Neutron Diffraction Powder Patterns Modified for Anisotropic Thermal Vibrations*, UKAERE Harwell Rep. RRL 73/897, Harwell 1973.
17. Rietveld, H. M. *J. Appl. Crystallogr. 2* (1969) 65.
18. Koester, L. and Yelon, W. B. In: Yelon, W. B., Ed., *Neutron Diffraction Newsletter*, The Neutron Diffraction Commission, Missouri 1983.
19. Watson, R. E. and Freeman, A. F. *Acta Crystallogr. 14* (1961) 27.
20. Zener, C. *Phys. Rev. 82* (1951) 403.
21. Anderson, P. W. and Hasegawa, H. *Phys. Rev. 100* (1955) 675.
22. de Gennes, P.-G. *Phys. Rev. 118* (1960) 141.

Received April 22, 1992.